VARIABILITY OF BOW SHOCK LOCATION AT MARS

Yu Yi, Eojin Kim, Yong Ha Kim[1], Jhoon Kim[2]
[1]Department of Astronomy and Space Science, Chungnam National University Taejon 305-764
E-mail: euyiyu@hanbat.chungnam.ac.kr, yhkim@hanbat.chungnam.ac.kr
[2]Korea Aerospace Research Institute
E-mail: jkim@kari.re.kr

ABSTRACT

Bow shock formation, in case the supersonic solar wind flow is hindered by the atmosphere of Mars, is investigated. The atoms newly ionized from the extensive neutral atmosphere of Mars are loaded to the solar wind. By the conservation of momentum, the solar wind velocity is decreased. Then the supersonic flow velocity drops to the subsonic flow velocity in front of Mars at certain region, which is called the bow shock. The location of Mars subsolar bow shock is highly varying in the range of 1.3 to 2.5 R_m. Martian bow shock location is estimated by one-dimensional flux tube equations reduced from full three-dimensional MHD equations. The variability of Mars bow shock location effected by the solar wind conditions is studied. It is evident that the solar wind dynamic pressure change is able to make the Mars bow shock location variable.

1. INTRODUCTION

1.1 Solar wind Interaction with Mars

The type of interactions between the supersonic solar wind and the planets in the solar system is categorized into two cases. In the case of strongly magnetized planets such as Earth, Jupiter, and Saturn, the solar wind is obstructed by the intrinsic magnetic field of the planets outside the planetary ionosphere. However, in the case of the planets unmagnetized but possessing fairly thick ionosphere such as Mars, Venus, and comets, the solar wind flow is hindered by the unshielded ionosphere. In both cases, the interaction with the solar wind forms a characteristic boundary called the bow shock.

In the latter interaction, the dominant process is called mass loading of planetary ions to solar wind. In this mass loading process, the ions newly produced by the ionization of the extensive neutral atmosphere is picked up by the solar wind magnetic field. Conservation of momentum requires that this kind of mass addition to the solar wind results in a decrease of its velocity. This mass loading process contributes to formation of the bow shock.

1.2 Exploration of Mars

The bow shock locations near Mars were observed by the spacecraft Mariner 4 in 1964, Mars 2 and 3 in 1972, Mars 5 in 1974, and Phobos 2 in 1988. These missions to Mars have established
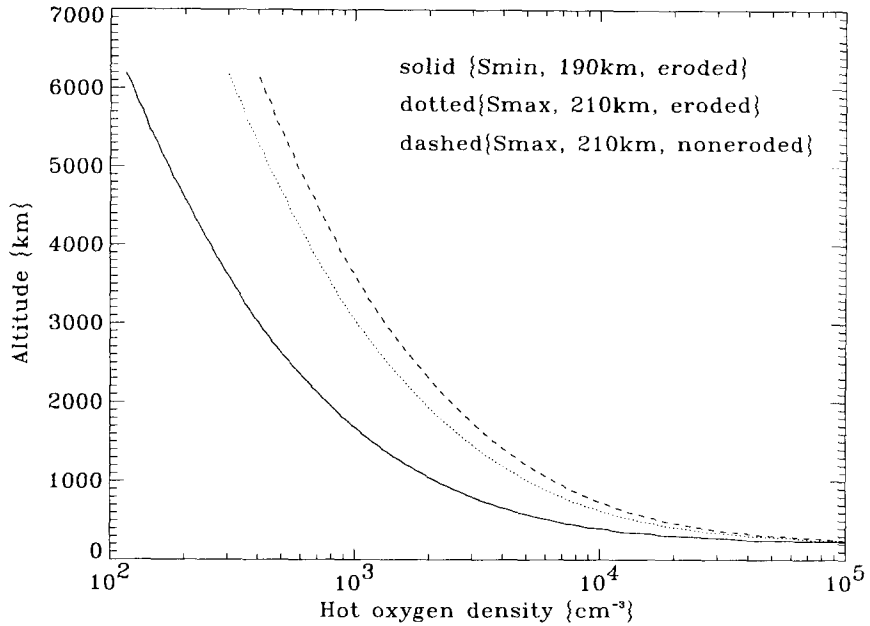
Figure 1. Hot oxygen density profiles for high and low solar cycle conditions, calculated by Kim et al. (1998)

the existence of an ionosphere, and a magnetotail as well as a bow shock. Even though the poor statistics in the number of crossings of the bow shock led to uncertainty in its shape and in its altitude at the subsolar point, these values are important for estimating the contribution of the Martian upper atmosphere to the interaction with the solar wind. Slavin et al.(1991) showed the locations of bow shock detected by above five spacecraft. The modeling results from all spacecraft data show that the range of subsolar bow shock distance is 1.3 to 2.5 R_m.

1.3 Modeling of Mars

MHD model is crucial for the analysis of data collected by Mars exploration spacecraft in the past and in the future. Recently a couple of MHD models of Mars interacting with the solar wind have been developed (Liu et al. 1999 and Kim et al. 1999). MHD model is able to explain the significance of mass loading for the structure of ionosphere including locations of the bow shock and the magnetic barrier. Three-dimensional simulation models are useful in figuring out the global structure of Mars magnetosphere. However, three-dimensional simulation has its own shortcomings. It can not reduce the grid size as smaller as required to describe the discontinuities such as the bow shock due to economy of memory storage and computation time. Even though both Liu et al. (1999)
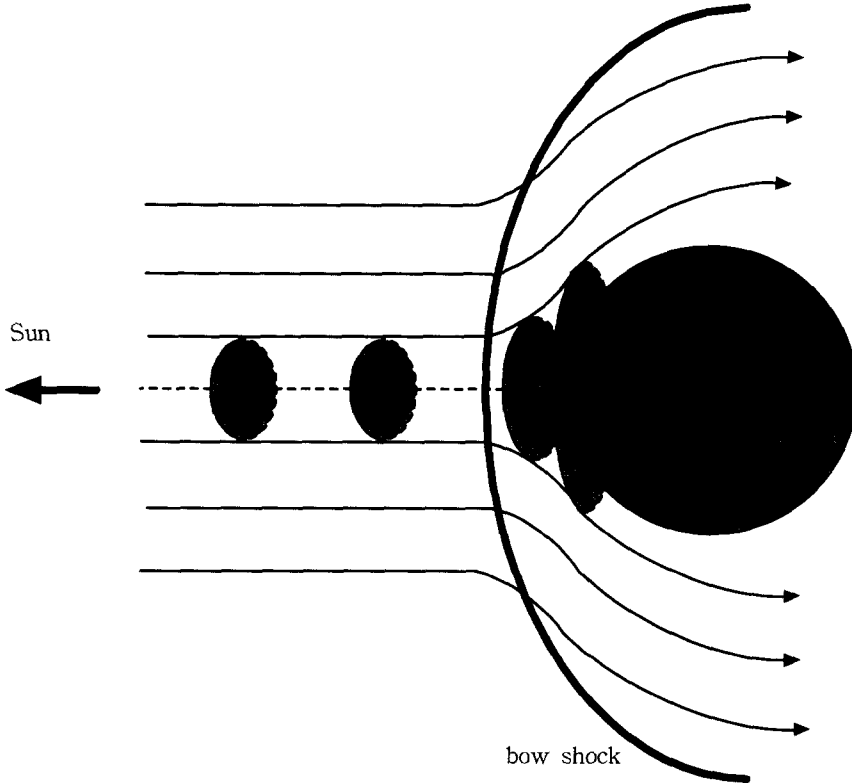
Figure 2. Schematic diagram of the solar wind - Mars interaction. The diagram is not to scale.

and Kim et al. (1999) were able to show the global structures of Mars, their grid sizes at the position of bow shock were 425 km and 120 km, respectively. Considered that numerical simulation diffuses the shock discontinuity over three or four grid space due to numerical diffusion, it is required that the grid space at the shock should be less than 100 km to describe the Mars bow shock whose thickness is about 250 km (Kallio, 1996). However, one-dimensional calculation can design any grid space without worrying about computation resources. Thus, since our main purpose of research is bow shock location at the subsolar point one-dimensional MHD flux tube calculation is done as our step forward into researches on Mars.

For the MHD modeling of martian bow shock and the ionosphere, the neutral atmosphere model is required as a ionization source. The neutral atmosphere have been modeled already by Kim et al. (1998). They have already calculated the distribution of the hot oxygen corona at Mars as a function of altitude up to 6,000 km above the Mars surface.
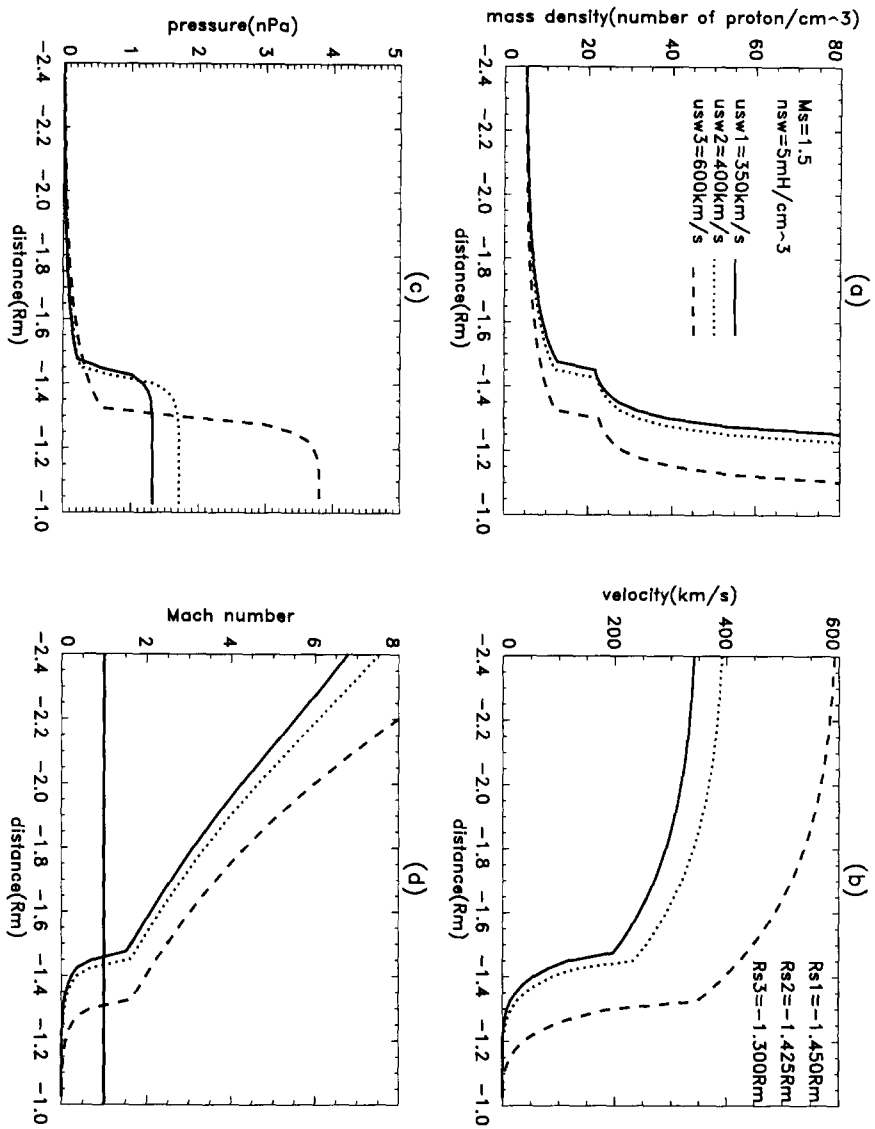
Figure 3. Profiles of (a) the mass density, (b) flow velocity, (c) plasma pressure, and (d) sonic Mach number along the Sun-Mars axis in four cases of solar wind velocities set as 350, 400, and 600 km/sec. The corresponding bow shock locations in subsolar direction are 1.450, 1.425, and 1.300 R_m , respectively.

2. MHD model of bow shock formation

The ideal compressible MHD equations with ion source term q outflowing with velocity w can be written as follows: Mass conservation

$$\frac{\partial \rho}{\partial t} = -\nabla \cdot (\mathbf{v}\rho) + q \tag{1}$$

Momentum conservation

$$\frac{\partial (\rho \mathbf{v})}{\partial t} = -\nabla \cdot [\rho \mathbf{v}\mathbf{v} + P\hat{\mathbf{I}} - \frac{1}{\mu_0}(\mathbf{B}\mathbf{B} - \frac{1}{2}B^2\hat{\mathbf{I}})] + q(\mathbf{w} - \mathbf{v}) \tag{2}$$

Energy conservation

$$\frac{\partial U}{\partial t} = -\nabla \cdot S + \frac{\gamma - 1}{2}q(\mathbf{w} - \mathbf{v})^2 \tag{3}$$

$$U = \frac{1}{2}\rho v^2 + \frac{P}{\gamma - 1} + \frac{B^2}{2\mu_0}$$

$$S = \left[U + P + \frac{B^2}{2\mu_0}\right]\mathbf{v} - \frac{(\mathbf{v} \cdot \mathbf{B})\mathbf{B}}{\mu_0}$$

Faraday's law

$$\frac{\partial \mathbf{B}}{\partial t} = \nabla \times (\mathbf{v} \times \mathbf{B}) \tag{4}$$

where ρ is the plasma mass density, v the plasma flow velocity, P the plasma pressure, B the magnetic field, and γ the ratio of specific heat (here γ is set 5/3 by assuming the adiabatic process for the ideal monoatomic gas) [Min et al., 1985]. The solar wind particle and Mars originated ions are not distinguishable in this single fluid MHD calculation.

2.1 One-dimensional flux tube calculation

Assuming the steady state, one-dimensional calculation of conservation equations of mass, momentum, and energy fluxes along a stream tube of cross section A on the sun-Mars axis can be reduced from three-dimensional MHD equations. Considering only $\mathbf{B} = B\hat{y}$ and $\mathbf{v} = v\hat{x}$ components, those equation can be written as

$$\frac{1}{A}\frac{d}{ds}(\rho u A) = q \tag{5}$$

$$\frac{1}{A}\frac{d}{ds}(\rho u^2 A) + \frac{d}{ds}(P + \frac{B^2}{2\mu_0}) = 0 \tag{6}$$

$$\frac{1}{A}\frac{d}{ds}\left[uA\left(\frac{1}{2}\rho u^2 + \frac{\gamma p}{\gamma - 1} + \frac{B^2}{\mu_0}\right)\right] = 0 \tag{7}$$

$$\frac{1}{A}\frac{d}{ds}(uBA) = 0 \tag{8}$$

where s measures the distance along subsolar direction of Sun to Mars. Even though for a further simple analysis, the magnetic field B is not considered in current calculation, three equations (5) to (7) without B should be solved simultaneously. In this reduction, it is assumed that the mass source is dominant but the momentum and energy sources are neglected, since Biermann et al. (1967) showed that to a good approximation it is sufficient to include the mass loading effect in the mass density continuity equation but it can be neglected in the momentum and energy equations.

One-dimensional flux calculation delivers almost mathematically analytic solution without numerical noise and numerical diffusion intrinsic in a full three-dimensional MHD simulation. Currently this approach is mainly interested in the variation of bow shock location along the subsolar direction. Thus one-dimensional flux tube calculation is much economical in computation and allows fast estimation of profiles of physical parameters such as mass density and pressure and flow velocity. This kind of approach has been successfully applied to the interaction between the solar wind and the comet by Ip (1980), but never to Mars. It is expected that this reduced one-dimensional approach would results in the location of Mars bow shock closer to Mars compared to the three-dimensional simulation since momentum and energies are taken out in the process of simplification.

The hot oxygen corona around Mars is the significant neutral constituent for ion production effective in mass loading to the solar wind since other thermal components only contribute at the lower atmosphere not related to the formation of the bow shock. Even though no observation of the hot oxygen population is available to date, the hot oxygen corona density profile, calculated by Kim et al. (1998) shown in Figure 1, is used. The neutral hot oxygen atmosphere density distribution function in Equation (9) is taken as an approximation of solar maximum case in Figure 1:

$$N(r) = N_{eb} \times \exp\left[-\frac{(r - r_0)}{hs}\right] \tag{9}$$

where the r_0 = 3700 km was radius of exosphere base, which is 300km above Mars surface, h_s =1,000 km is the scale height of hot oxygen density profile, and $N_e b = 3.0 \times 10^5 cm^-3$ number of hot oxygen density at the exosphere base.

Only photoionization by solar UV radiation is considered as an unique ionization mechanism. The ion source function is taken as q(r) = $\sigma \times$ N(r) , where $\sigma = 10^{-6}$/sec is the ionization rate by solar UV radiation and the N(r) is the neutral hot oxygen density distribution given in equation (9).

For a simple and analytic solution, it was assumed that in the supersonic flow region before the shock , it was set A=constant and in the subsonic flow region after the shock, vA=constant. The schematic diagram shown in Figure 2 might be helpful in understanding this assumption. This assumption may not be valid either at the lower ionosphere or in the region far off-axis from the Sun-Mars line but is only valid enough at the high ionosphere just inside of Mars bow shock along the subsolar direction. Thus, it is sufficient for estimating the bow shock location with ease. At the position of the shock, the Rankine-Hugoniot relations were applied. Using the subscript 1 and 2 for the values of the variables immediately before and behind the shock. The relations between the variables before and after the shock on the axis are written as:

$$\rho_2 = \rho_1 \left[\frac{1}{1 - \frac{2}{\gamma+1}\left(1 - \frac{1}{M_1^2}\right)} \right] \qquad (10)$$

$$u_2 = u_1 \left[1 - \frac{2}{\gamma+1}\left(1 - \frac{1}{M_1^2}\right) \right] \qquad (11)$$

$$P_2 = P_1 \left[1 + \frac{2\gamma}{\gamma+1}(M_1^2 - 1) \right] \qquad (12)$$

Given the solar wind parameters and ionization source term, the quantities of density, pressure and velocity were calculated step by step by one-dimensional flux tube equations (5) to (7). The calculation was carried out from 2.5 R_m to 1.1 R_m by 85 km in grid space. Starting from 2.5 R_m, supersonic solutions were sought. If the Mach number reached a certain value set initially, then Rankine-Hugoniot relations of equations (10) to (12) were applied at the shock boundary. After crossing the bow shock the subsonic solutions were figured out. The given initial solar wind parameters are: solar wind velocity v=350 km/sec, solar wind proton density 5 m_H/cm^3, solar wind plasma pressure p=6.9 $\times 10^{-3} nP_a$, which means that the solar wind temperature is 10^5 K.

3. Results and Discussions

The three-dimensional MHD simulation estimated in a preshock Mach number of 1.5 to 2.0 dependent on the definition of shock discontinuity over three grid or four grid spaces. (Kim et al. 1999). Mars has a weaker bow shock. Thus, the dependency of bow shock location on solar wind conditions is studied with preshock Mach number, which means the Mach number at the front of upstream shock boundary, set as 1.5. in the following calculations.

First, the solar wind dynamic pressure effect is tested by three kinds of solar wind velocities of 350, 400, and 600 km/sec with solar wind density of 5 m_H/cm^3. Profiles of (a) the mass density, (b) flow velocity, (c) plasma pressure, and (d) sonic Mach number along the subsolar direction are shown in Figure 3. At the bow shock, the mass density and plasma pressure and flow velocity change with the discontinuities. Crossing the bow shock boundary from upstream to downstream, the plasma density and pressure jump up and the flow velocity drops below 100 km/sec. The locations of bow shock are 1.450, 1.425 and 1.300 R_m, respectively. The higher solar wind velocity pushes Mars bow shock location inward. Second, the similar calculation is performed by changing the solar wind density. Figure 4. shows profiles of (a) the mass density, (b) flow velocity, (c) plasma pressure, and (d) sonic Mach number in three cases of solar wind density of 5, 10, 15 m_H/cm^3 with the solar wind velocity 350 km/sec fixed. Bow shock positions are estimated at 1.450, 1.250, and 1.125 R_m, respectively. The denser solar wind moves Mars bow shock location back toward the Mars surface.

In addition, the dependency of bow shock location on the strength of the bow shock is tested in four cases of preshock Mach number of 1.3, 1.5, 2.0, and 3.0 with given solar wind velocity 350 km/sec and density 5 m_H/cm^3. The calculated profiles of the mass density, flow velocity, plasma pressure, Mach number of each cases are shown in Figure 5. The corresponding positions
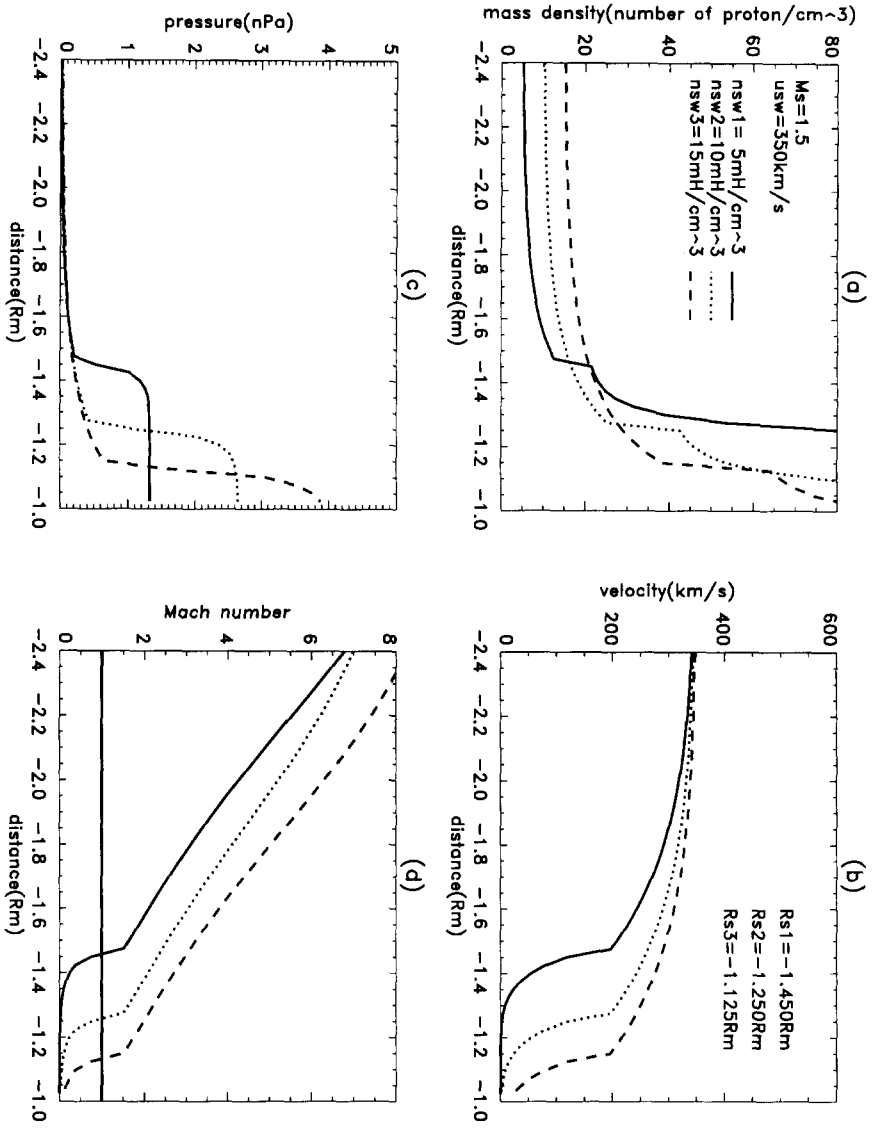
Figure 4. Profiles of (a) the mass density, (b) flow velocity, (c) plasma pressure, and (d) sonic Mach number along the Sun-Mars axis in four cases of solar wind densities set as 5, 10, 15 m_H/cm^3. The bow shock locations at 1.450, 1.250, and 1.125 R_m corresponds to each solar wind densities.
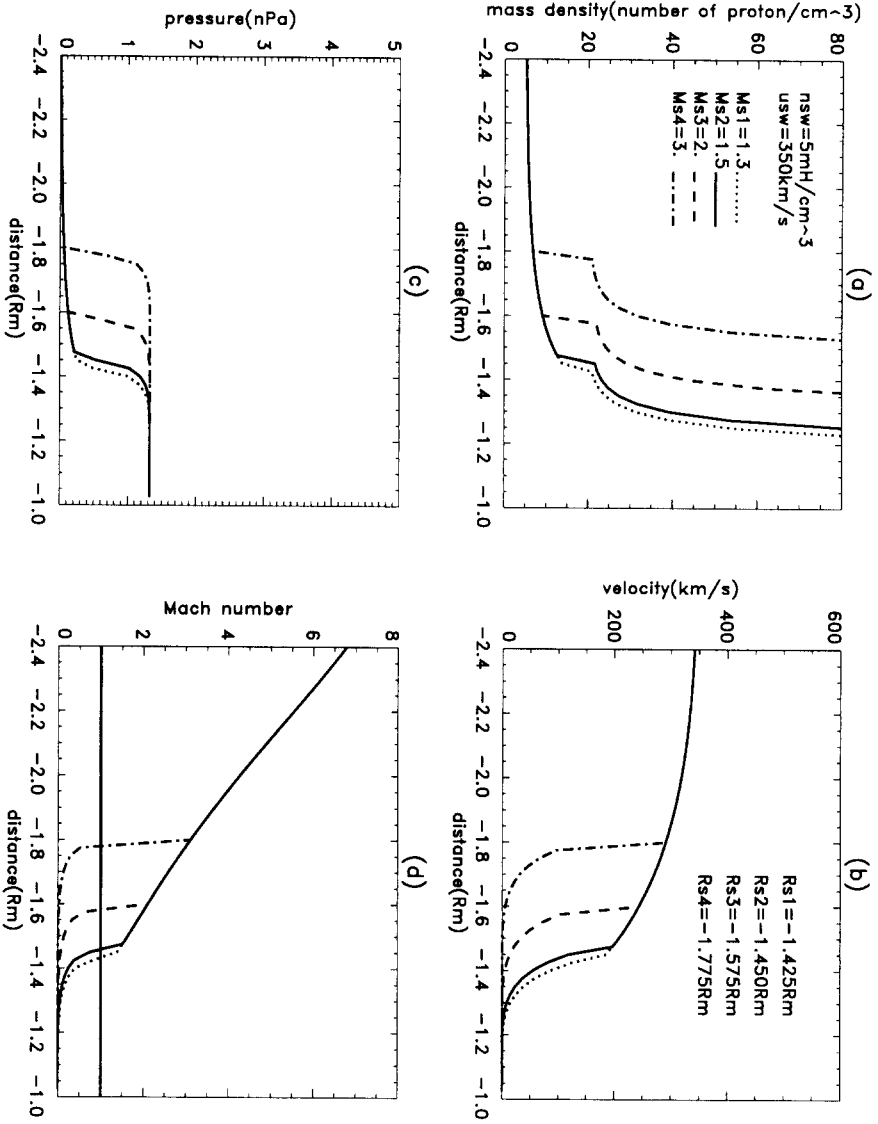
Figure 5. Profiles of (a) the mass density, (b) flow velocity, (c) plasma pressure, and (d) sonic Mach number along the Sun-Mars axis in four cases of preshock Mach number set as 1.3, 1.5, 2.0, and 3.0.

of subsolar bow shock are 1.425, 1.450, 1.575, and 1.775 R_m in order. The stronger the bow shock represented by the higher preshock Mach number, the further out the position of the bow shock moves. If the preshock Mach number were set 2.0 or over, the shock would be settled farther out from Mars. Those numbers are reasonable considered that the relatively strong bow shock of comet Halley whose preshock Mach number is over 3.2 (Yi et al. 1996).

It is evident that highly varying Mars bow shock location is well explained by the solar wind dynamic pressure change. However, it may be possible that the Mars bow shock location would not vary as much as expected by solar wind dynamic pressure change. If the solar wind dynamic pressure increases, it will move the bow shock location inward to Mars. However, the preshock Mach number may increase in reaction against it, then the shock moves back outward.

Further researches are currently on going for improvement in this flux tube model. The solutions of four equations including Faraday's law of magnetic field B should be sought for constructing the realistic MHD model. The multi-components atmosphere model including thermal oxygen and hydrogen and hot hydrogen as well as the hot oxygen will be used for more sophisticated model calculation. The neutral atmosphere composed of four components modeled by Nagy et al. (1990) is available for the upgrade of current model. The bow shock location is determined by many factors such as not only the atmosphere density but also total ionization rate through many other ionization processes. Thus, the dependency of bow shock location on the variations of all those effects should be studied step by step.

REFERENCES

Biermann, L., B. et al., 1967, Solar Physics, 1, 254.

Ip, W.-H., 1980, ApJ, 238, 388-393.

Liu, Y. et al. 1999, GRL, 26, 2689-2692.

Kallio, E., 1996, JGR, 101, 11133-11147.

Kim, E., Y. Yi, Y. H. Kim, and J. Kim, 1999, Structure of Martian Magnetosphere, presented at 1999 Spring meeting of the Korean Space Science Society and submitted for the publication in JKAS, 32(2).

Kim, J., et al., 1998, JGR, 103, 29339-29342.

Min, K. H., et al., 1985, JGR, 90, 4035-4045.

Nagy et al., 1990, Annales Geophysicae, 8, 251-256.

Slavin et al., 1981, JGR, 96, 11235-11241.

Yi et al., 1996, JGR, 101, 27,585-27,601.